



Influence of glacial isostatic adjustment on river evolution along the U.S. mid-Atlantic coast

T. Pico^{a,*}, J.X. Mitrovica^a, J.T. Perron^b, K.L. Ferrier^c, J. Braun^d

^a Department of Earth and Planetary Sciences, Harvard University, Cambridge, MA, USA

^b Department of Earth, Atmospheric, and Planetary Sciences, Massachusetts Institute of Technology, Cambridge, MA, USA

^c Department of Geoscience, University of Wisconsin, Madison, WI, USA

^d GFZ Deutsches GeoForschungszentrum and University of Potsdam, Potsdam, Germany

ARTICLE INFO

Article history:

Received 18 February 2019

Received in revised form 30 May 2019

Accepted 22 June 2019

Available online xxx

Editor: J.P. Avouac

Keywords:

glacial-isostatic adjustment

U.S. east coast river geomorphology

river dynamics on glacial timescales

ABSTRACT

Long-term river evolution depends partly on crustal deformation, which shapes the topography crossed by rivers. On glacial timescales, ice-sheet growth and decay can produce crustal vertical motion of ~ 10 mm/yr resulting from the solid Earth's adjustment to variations in ice and water loads, comparable to tectonically-driven rates in the most rapidly uplifting mountains on Earth. This process of glacial isostatic adjustment (GIA) can influence river courses and drainage basins substantially, particularly near former ice margins. We explore the extent to which GIA influenced the evolution of rivers along the United States east coast during the last glacial cycle. We compute gravitationally self-consistent GIA responses that incorporate recent constraints on the Laurentide Ice Sheet history through the last glacial build-up phase, and we connect the predicted variations in topography to abrupt changes in river dynamics recorded in the Hudson, Delaware, Susquehanna, and Potomac Rivers from 40 ka to present. To the extent that increases in sediment transport capacity imply increases in river incision rate, the GIA-driven changes in slope and drainage area are consistent with episodes of erosion and sedimentation observed in the Hudson, Delaware, and Potomac Rivers, but inconsistent with the observed accelerated river incision in the Susquehanna River at 30–14 ka. These analyses add to a growing body of evidence showing that GIA strongly influences river evolution over millennial timescales.

© 2019 Elsevier B.V. All rights reserved.

1. Introduction

The growth and decay of continental ice sheets deform the solid Earth on the $\sim 10^5$ -year timescales associated with Late Pleistocene glacial-interglacial cycles. This process has produced up to 10 mm/yr of crustal vertical motion hundreds of kilometers away from Late Pleistocene ice cover (Whitehouse et al., 2007), matching or exceeding tectonic rock uplift rates in these regions (i.e. Moucha et al., 2008). Previous studies show that this process of glacial isostatic adjustment (GIA) produces sufficient crustal deformation to control rates of river incision (Wickert et al., 2019), river drainage patterns (Wickert, 2016), river diversions (Pico et al., 2018b), and delta accumulation rates (Whitehouse et al., 2007).

Because ice sheets blanketing North America contained the largest excess ice volume at the Last Glacial Maximum (LGM, 26–20 ka; Clark et al., 2009), the U.S. east coast experienced high rates of GIA-induced crustal deformation (~ 10 mm/yr), as it is located on the formerly uplifted region, or peripheral bulge, surrounding the Laurentide Ice Sheet. The eastern Laurentide Ice Sheet began growing rapidly around 50–35 ka, according to inferences from sea-level markers along the U.S. mid-Atlantic coast (Pico et al., 2017), and initiated uplift along the U.S. east coast as the solid Earth adjusted to an expanding ice load. During the peripheral bulge growth phase, various rivers along the U.S. east coast, including the Hudson, Potomac, Susquehanna, and Delaware, experienced major changes in their evolution. Although deglaciation was rapid after the LGM, the eastern sector of the Laurentide Ice Sheet remained a major ice load until the early Holocene (~ 11 ka; Dyke, 2004), such that subsidence rates from 20 to 10 ka in the U.S. mid-Atlantic region were slower than GIA-induced uplift rates during the peripheral bulge growth phase. Here we investigate the potential role of GIA-driven crustal deformation in the evolution of these four major rivers on the U.S. Atlantic coastal plain.

* Corresponding author.

E-mail address: tpico@g.harvard.edu (T. Pico).

2. Background

2.1. U.S. east coast rivers during peripheral bulge growth

Transitions in river dynamics are recorded in the Hudson, Delaware, Susquehanna, and Potomac Rivers during the period ~40–10 ka. In the ancestral Hudson River, sediment cores and seismic reflection surveys record an eastward diversion at ~30 ka (Carey et al., 2005; Knebel et al., 1979). Sediment cores sampling fluvial deposits in the lower reaches of the Delaware River record a switch from incision to aggradation in an estuarine and organic-rich environment from 40 to 25 ka (Stanford et al., 2016). Stanford et al. (2016) argue that the Delaware River fully diverted eastward to the Raritan drainage basin after 25 ka based on correcting the shallow present-day profile of the Delaware River with a linearly projected forebulge reconstructed from proglacial lake shorelines. In contrast to aggradation in the Delaware, an incisional pulse occurred in the Susquehanna and Potomac Rivers from 30 to 14 ka and 33 to 13 ka, respectively, with erosion rates more than doubling compared to those in the previous interval (Bierman, 2015; Reusser et al., 2006, 2004). Reusser et al. (2006) argue that this pulse of incision reflected a wider regional change in river dynamics rather than an increase in glacial meltwater flux, given that erosion rates in the partly glaciated Susquehanna and the unglaciated Potomac were comparably high during the incision pulse.

Each of these transitions – whether a diversion or a change in the rate of incision or aggradation – has been interpreted as a consequence of crustal deformation associated with the growth of the peripheral bulge of the Laurentide Ice Sheet. Studies of the Delaware and Hudson River have speculated that the peripheral bulge played an important role in the shift to aggradation in the Delaware (Stanford et al., 2016) and the eastward diversion of the Hudson (Knebel et al., 1979). Pico et al. (2018b) forced a landscape evolution model with numerical predictions of GIA and found that crustal uplift caused by a rapid growth of the Laurentide Ice Sheet is consistent with an eastward diversion of the Hudson River at ~30 ka. The high incision rates in the Potomac and Susquehanna from ~30 to 15 ka have been qualitatively linked to regional changes in precipitation, rapid base-level fall, or uplift of the peripheral bulge (Reusser et al., 2006).

Here we test whether GIA can quantitatively explain the observed trends in river regime (incision vs. aggradation) in the Susquehanna, Potomac and Delaware Rivers. We reconstruct topography based on GIA simulations to determine changes to river channel slope and drainage area in each of these rivers. We then estimate the resulting perturbation to sediment transport capacity and compare these changes to the recorded changes in sedimentation and erosion rates.

2.2. GIA and ice history constraints from 120 to 26 ka

The growth and decay of continental ice sheets drive a complex pattern of sea-level (or equivalently topographic) change. In the simulations discussed herein, we perform GIA calculations based on the theory and pseudo-spectral algorithm described by Kendall et al. (2005) with a spherical harmonic truncation at degree and order 256. These calculations include the impact of load-induced Earth rotation changes on sea level (Milne and Mitrovica, 1996) as well as evolving shorelines and the migration of grounded, marine-based ice (Kendall et al., 2005; Lambeck et al., 2003). Our predictions require models for Earth's viscoelastic structure and the history of global ice cover. We use an Earth model with upper and lower mantle viscosities of 0.5×10^{21} Pa s and 1.5×10^{22} Pa s, respectively; these values are consistent with inferences from GIA analyses of sea-level highstands along the U.S. mid-Atlantic extend-

ing from Marine Isotope Stages (MIS) 5 to 3 (Creveling et al., 2017; Pico et al., 2017; Potter and Lambeck, 2003).

A major challenge in selecting an ice history across the glacial build-up phase is the sparsity of geologic data constraining global mean sea level (GMSL) and continental ice extent. During the glacial build-up phase, global sea level was lower than it is today, and subsequent sea-level rise during the last deglaciation (26 ka to present) destroyed or submerged the majority of sea-level records. In addition, as the Laurentide Ice Sheet grew to its maximum extent at the LGM, it destroyed most evidence of prior ice margins (Dyke et al., 2002). Recent GIA modeling studies have refined the pace of global sea-level fall leading into the LGM (Pico et al., 2016), and an analysis of sea-level data on the U.S. east coast (Pico et al., 2017) supports field evidence for a late and rapid glaciation of the eastern sector of the Laurentide Ice Sheet (Dalton et al., 2016; Carlson et al., 2018). In the following simulations we revise the standard ICE-5G ice history (Peltier and Fairbanks, 2006; black line in Fig. 1C) in accordance with these recent analyses to construct an ice model we term ICE-PC2. We use a peak GMSL value during MIS 3 of -37.5 m at 44 ka (Pico et al., 2016). Second, we use GMSL values of -15 m and -10 m for MIS 5a (80 ka) and 5c (100 ka), respectively; these values are within bounds (5a: -18 m to 0 m, 5c: -20 m to 1 m) derived by Creveling et al. (2017) on the basis of globally distributed sea level markers from both periods (blue; Fig. 1B). Finally we require that the eastern section of the Laurentide Ice Sheet is ice-free from 80 to 44 ka, and grows rapidly to its LGM extent as in Pico et al. (2018a). GIA simulations are primarily sensitive to total loads, and therefore predictions for the U.S. east coast are robust to changes in the ice margin geometry of ICE-PC2.

Our aim is to determine the extent to which GIA processes, in particular the growth of the peripheral bulge of the Laurentide Ice Sheet, exerted control on the abrupt transitions in river dynamics recorded during the last glacial cycle along the U.S. east coast. We model GIA-corrected topography during the interval when major geomorphic changes are recorded in U.S. mid-Atlantic rivers. Specifically, we use ice history ICE-PC2 and focus on topographic changes from 36 to 20 ka, as this period encompasses maximum rates of crustal deformation due to the growth of the peripheral bulge of the Laurentide Ice Sheet. These rates are characterized by a general north-south gradient in uplift, in addition to lateral variations caused by the distribution of ice lobes and the effect of ocean loading near the coasts (Pico et al., 2018b). Ice lobes extending south from the main Laurentide Ice Sheet represent local loads that superimpose smaller peripheral bulges on the longer wavelength peripheral bulge that extends across the entire United States (Fig. 1A).

3. Methods: GIA effects on river channels

The tendency of a riverbed to erode or aggrade depends on the sediment transport capacity of the river (Q_c) relative to the sediment supply from upstream (Q_s). If the transport capacity of a river reach exceeds the upstream sediment supply, the bed will erode. If the upstream sediment supply exceeds the transport capacity, the bed will aggrade. Both sediment supply and transport capacity may have varied in U.S. mid-Atlantic rivers from 36 to 20 ka during the time interval of peripheral bulge growth. For example, changing patterns of glacial and periglacial erosion could have altered sediment supply volume or grain size through time, and changing precipitation patterns (and ice melting, in the case of glaciated basins) could have altered sediment transport capacity. Given the lack of detailed information about sediment supply and climate variability from 36 to 20 ka in the study region, we focus on perturbations to sediment transport capacity associated with GIA, and neglect changes in sediment supply or precipitation-induced changes in sediment transport capacity. Our goal is to test

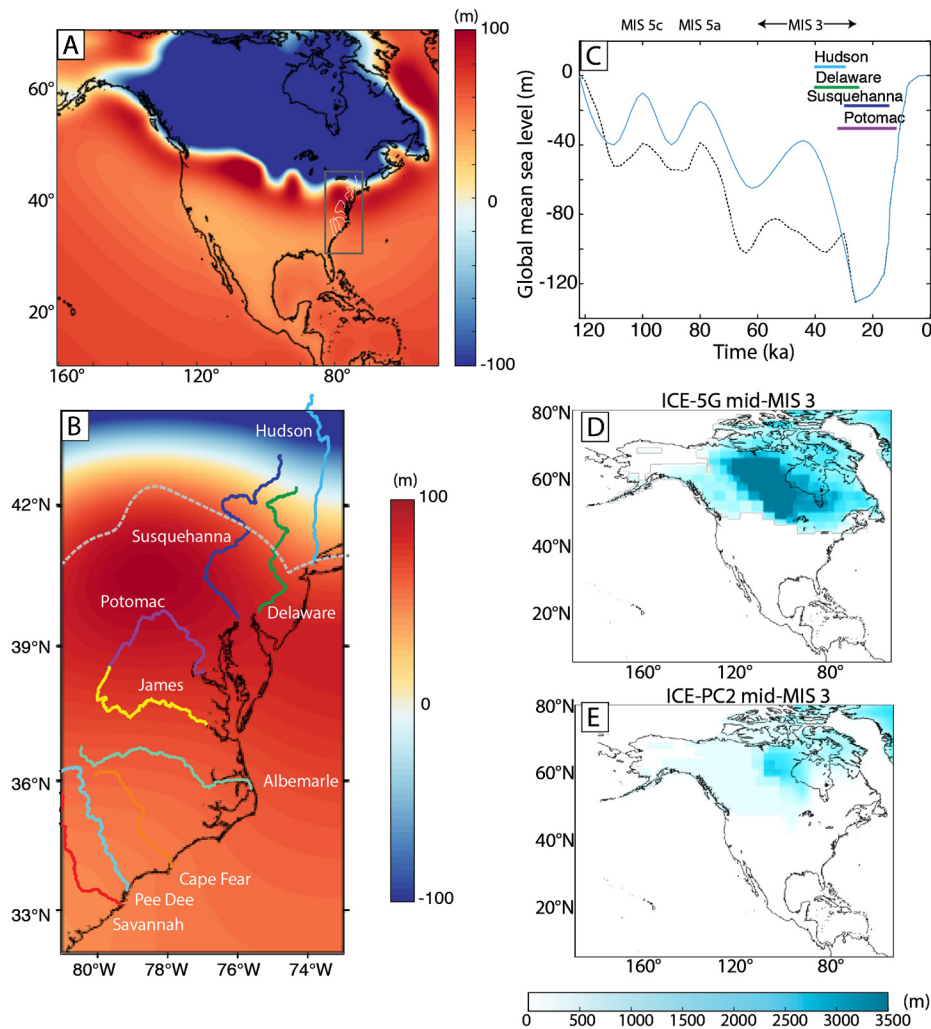


Fig. 1. (A) Predicted topographic changes from 36 to 20 ka using ice history ICE-PC2 (uplifted regions in red) over North America. Rectangle indicates the region shown in (B), where major U.S. east coast rivers are labeled. The approximate extent of ice at the Last Glacial Maximum is shown by the dashed gray line. (C) Global mean sea level history for ice history ICE-5G (dotted black) and ICE-PC2 (blue). Horizontal lines indicate dates of observed river dynamic changes in labeled rivers. Remaining two frames show the geographic extent of ice at 44 ka (mid-MIS 3) in (D) ICE-5G and (E) ICE-PC2. (For interpretation of the colors in the figure(s), the reader is referred to the web version of this article.)

whether modeled GIA-induced changes in transport capacity can explain the sign of observed changes in fluvial sedimentation (erosion vs. aggradation).

3.1. Effects of slope and drainage area on sediment transport capacity

The sediment transport capacity Q_c of a river reach depends on the bed shear stress. In studies of long-term river profile evolution, it is common to use expressions for runoff, river channel hydraulic geometry, and steady, uniform open-channel flow of an effective water discharge to relate the bed shear stress to the upstream drainage area (A) and the local channel bed slope (S), yielding (e.g., Willgoose et al., 1991; Howard et al., 1994)

$$Q_c = kA^m S^n, \quad (1)$$

where k is a transport coefficient and the exponents m and n are constants. We assume that k , m and n remain constant in space and time and use GIA-driven changes in slope and drainage area to calculate the perturbation to sediment transport capacity Q_c for each river from 36 to 20 ka. The right-hand side of Equation (1) has the same form as the channel incision rate in the stream power equation for bedrock channel incision (Howard and Kerby, 1983; Seidl and Dietrich, 1992; Whipple and Tucker, 1999).

We therefore use the product $A^m S^n$ as a generic proxy for either sediment transport capacity or bedrock incision rate. For cases in which a bedrock channel experienced a change in incision rate, we set $m = 0.5$ and $n = 1$, consistent with estimated values worldwide that typically put m/n close to 0.5 (Harel et al., 2016) and more generally in the range 0.35–0.6 (Whipple and Tucker, 1999). For cases in which a channel experienced aggradation or erosion of sediment, we set $m = 1.5$ and $n = 1$, consistent with field data (e.g., Massong and Montgomery, 2000) and with previous estimates that suggest $(m - 1)/n \approx 0.5$ for transport-limited channels (Whipple and Tucker, 2002).

The stream power model that we apply in cases of bedrock incision does not account for erosion thresholds or sediment abrasion dynamics, both of which may influence the rate of river incision (Sklar and Dietrich, 2001, 2004; Snyder et al., 2003; Whipple, 2004; Yanites, 2018). A threshold shear stress for bedrock erosion may affect the magnitude of the river channel response to a particular change in slope or drainage area, but it should not change the fact that an increase in slope or drainage area will generally increase the time-averaged incision rate. Erosion by bedload abrasion may depend on grain size and sediment supply such that erosion rates generally increase with grain size and reach a maximum at an intermediate sediment supply

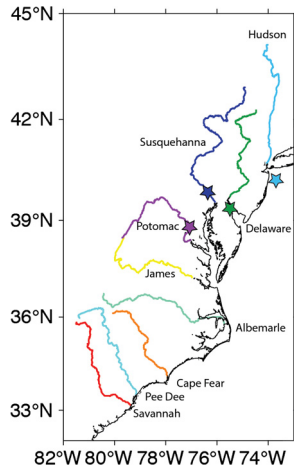


Fig. 2. A. Present-day channel paths of major rivers along the U.S. east coast. Locations of published observations of river changes at ~40-10 ka are shown by stars.

(Sklar and Dietrich, 2001, 2004). This too may influence the magnitude of the incision rate, and an increase in upstream drainage area could increase sediment supply enough to inhibit bedrock erosion. Ultimately, an increase in the ratio of sediment transport capacity to sediment supply should lead to faster incision or slower sediment aggradation.

To calculate the change in sediment transport capacity or bedrock incision rate from Equation (1), we first modeled the GIA-induced changes in river channel slope and drainage area for the rivers shown in Fig. 1A. We then calculated fractional changes in the sediment transport capacity or bedrock incision rate of these rivers during the growth of the peripheral bulge from 36 to 20 ka using the modeled changes in channel slope and drainage area (Equation (2)). For a change in transport capacity (Q_c), for example,

$$\frac{\Delta Q_c}{Q_{c,36 \text{ ka}}} = \frac{A_{20 \text{ ka}}^m S_{20 \text{ ka}}^n}{A_{36 \text{ ka}}^m S_{36 \text{ ka}}^n} - 1 \quad (2)$$

Although we use the quantity on the right-hand side of Equation (2) as a proxy for either a change in bedrock incision rate or a change in transport capacity, hereafter we refer to this quantity as $\Delta Q_c/Q_c$ for simplicity.

3.2. Calculating the impact of GIA on slope and drainage area

We used steepest-descent flow routing to identify river flow paths and compute drainage areas. We used the HydroSHEDS North America 30-second resolution void-filled DEM (Lehner et al., 2008) and filled lakes and depressions to obtain continuous paths of descent to the ocean (Barnes et al., 2014). We identified major rivers by tracing the steepest-descent directions along the path of maximum drainage area. Next, we extracted modern river profiles starting at the drainage divide for the Hudson, Delaware, Susquehanna, and Potomac (Fig. 2). We then calculated reconstructed river profiles at 36 and 20 ka by applying the same flow routing algorithms to the void-filled and sink-filled topography at 36 and 20 ka, where upstream distance was measured from the modern coastline, before and after the GIA-induced crustal deformation shown in Fig. 1A.

Predicted river channel locations varied from 36 to 20 ka as a result of GIA-induced topographic changes (Appendix Fig. A.1). Therefore, we sought to compare slopes and drainage areas on the respective channel location for each time. In the following calculations we used the upstream distance (measured from the modern coastline) to compare slope and drainage area changes.

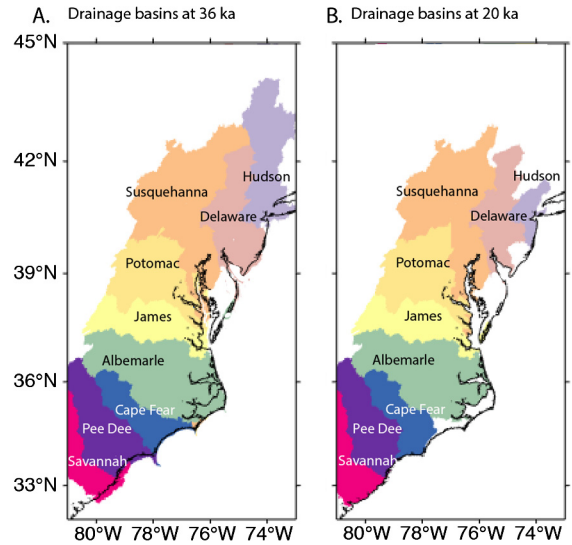


Fig. 3. Drainage basins at 36 ka (A) and 20 ka (B) using the reconstructed paleotopography driven by ice history ICE-PC2.

Then we mapped these changes onto the 36 ka river path (calculated starting from the modern coastline). Because the sinuosity of rivers may have changed from 36 to 20 ka, a given upstream distance may not represent the same location on both river channels. We compared the upstream distance on each location of the river channel, and showed that these differed by less than 10 km, except in the upper reaches of the Susquehanna and the Delaware (Appendix Fig. A.2). Some rivers, including the Albemarle, experienced small-scale avulsions or meanders in the modeled topography from 36 to 20 ka. These path changes have a small impact (<4 km) on the upstream distance calculated at each location (Appendix Fig. A.2), and comparing slopes at these sites can result in short-scale variations as the channel location switches.

3.3. Changes in slope

We used the modeled crustal deformation field shown in Fig. 1A to produce a map of the fractional change in river channel slope from 36 to 20 ka for all rivers in Fig. 2. First, we reduced noise associated with short-wavelength variations in the reconstructed topography by applying a 20 km-window smoothing filter to the river elevation profiles. We then calculated slope using a 10 km baseline and found the fractional change in slope from 36 to 20 ka as $(S_{20 \text{ ka}} - S_{36 \text{ ka}})/S_{36 \text{ ka}}$. Because the rivers turn sharply through the smooth field of GIA-induced topographic changes, our calculations indicate sudden changes in slope along the rivers in certain locations (Fig. 4A). The filtering we applied does not affect the GIA signal, since the smoothing window is considerably smaller than the wavelength of the GIA-induced crustal deformation field.

3.4. Changes in drainage area

We computed the percent change in drainage area along each river using the topography predicted from our GIA simulations at 36 ka and 20 ka. In Fig. 3 we present maps of drainage basins at 36 and 20 ka. To estimate total changes in drainage area due to GIA-induced deformation alone, rather than additionally including the effects of changes in drainage area due to coast migration resulting from sea-level change, we calculated the total drainage area at the shoreline predicted at 36 ka using ice history ICE-PC2 (Appendix Table A.1). At every location along the channel, we then calculated fractional changes in upstream drainage area as $(A_{20 \text{ ka}} - A_{36 \text{ ka}})/A_{36 \text{ ka}}$.

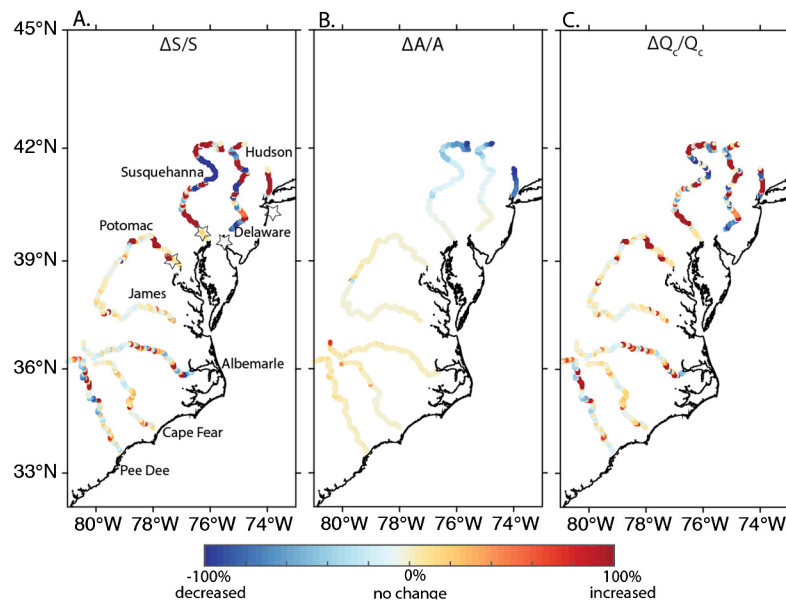


Fig. 4. GIA-induced percent changes from 36 to 20 ka in (A) channel slope (S) (B) drainage area (A) and (C) sediment transport capacity (Q_c), driven by ice history ICE-PC2 (Fig. 1A). Stars indicate locations of published observations of river changes at ~ 40 –10 ka.

4. Results & discussion: GIA effects on river channels

4.1. Impact of GIA on river channel slopes

Fig. 4A shows regions where the slope steepens (warm colors) and where slope shallows (cool colors). GIA-induced changes in slope are a result of the channel crossing through the crustal deformation field in Fig. 1A, in addition to changes in channel location, and are not simply correlated with proximity to the ice load.

While many stretches of rivers show little change in slope, with values close to 0%, several rivers show large percent differences in channel slope. In the Potomac River, channel slope increases significantly in the 100 km stretch upstream of the modern coastline (Fig. 4A). This includes a prominent peak within this stretch of river, where slope increases by 370%, corresponding well with the location ~ 25 km upstream of the modern coast where rapid erosion rates have been measured (Reusser et al., 2004).

In contrast to the GIA-driven increase in channel slope in the Potomac, the Delaware River channel slope shallows in the first 70 km upstream of the modern coastline (Fig. 4A). The slope decrease is -20% at the modern coastline, near the site in the Delaware Bay that records increased deposition (Stanford et al., 2016). The change in slope ranges from a maximum of -97% at a site 25 km upstream to 0% at a site 68 km upstream from the modern coastline. The Hudson River's slope is predicted to increase sharply, although the channel locations at 36 and 20 ka differ substantially (see Appendix Fig. A.1), since a portion of the Hudson's drainage basin was modeled as temporarily captured by another river during the growth of the peripheral bulge. Finally, we note there is no slope change in the Susquehanna near a location ~ 35 km upstream where increased incision rates were measured by Reusser et al. (2004). Instead, the modeled channel slope within the Susquehanna only changes starting 80–100 km upstream of the modern coastline (Fig. 4A), with slopes increasing by as much as 300%.

4.2. Impact of GIA on drainage area

Major reductions in drainage area occur along the Hudson, Delaware, and Susquehanna Rivers, (Fig. 4B), while the other rivers in the study area experience minor changes in drainage area. In

the case of the Hudson River, the total drainage area at the 36 ka coastline is reduced by a factor of 5, from 5.3×10^4 at 36 ka to 1.1×10^4 km² at 20 ka (Appendix Table A.1). This change in drainage area occurs because GIA-induced crustal deformation causes a large displacement of the drainage divide that defines the basin boundary (see Appendix Fig. A.1 for predicted channel locations at 36 and 20 ka; Fig. 3). The Susquehanna River total drainage area is similarly displaced by the growth of the peripheral bulge, although by only $\sim 7\%$, from 10.1×10^4 to 9.4×10^4 km² (Appendix Table A.1).

4.3. Impact of GIA on sediment transport capacity

We calculated changes to Q_c using Equation (2), based on the calculated changes to channel slope and drainage area (Fig. 4A/B). Fig. 4C shows a map of percent changes to Q_c for the rivers in Fig. 2.

Without estimates of sediment supply rate Q_s from 36 to 20 ka, we cannot quantify the magnitude of Q_c relative to Q_s , and therefore we cannot determine whether the study rivers were likely to have eroded or aggraded during this time period. However, we can gain insight by considering the simple scenario in which Q_c and Q_s are in balance at 36 ka everywhere along each river's length and in which Q_s remains steady from 36 to 20 ka. In this scenario, an increase in Q_c would imply a tendency to erode the riverbed, whereas a decrease in Q_c would imply a tendency to deposit sediment and aggrade. Under these conditions, the zones of increased transport capacity (warm colors in Fig. 4C) would be expected to have eroded from 36 to 20 ka, whereas the blue zones would be expected to have aggraded. Calculations using $m = 1.5$, the case associated with transport-limited channels, are shown in Appendix Fig. A.3. Changes to Q_c in the transport-limited case are only substantially different from the detachment-limited case in rivers with large changes in drainage area, because only in those cases does the different value of m have a substantial effect. We next discuss how our model calculations compare to existing observations for each river.

4.4. The Hudson and Delaware Rivers

Modeled transport capacity Q_c in the Hudson River sharply increases from 20 to 60 km upstream of the modern coastline,

though at the modern coastline modeled Q_c is reduced by 98% (Fig. 4C). Because the Hudson's drainage area is drastically reduced, it is the only river with substantially different results using the transport-limited exponents (Appendix Fig. A.3): in this case, modeled Q_c is reduced throughout the entire 0–80 km stretch upstream of the modern coastline. A modeled decrease in slope by 30% near the modern coastline is compounded by a drastic reduction of drainage area (Fig. 3). The latter result is consistent with a model of GIA-driven displacement of drainage divides throughout North America over the last deglaciation (Wickert, 2016). To the extent that reductions of both slope and drainage area imply an increased tendency to aggrade, this result is consistent with evidence of an eastward diversion of the Hudson River ~ 30 ka (Carey et al., 2005) given that increased aggradation would shallow slopes and make diversions more likely. On the other hand, it is possible that drainage area reduction lowered upstream sediment supply, a factor we do not consider here. Landscape evolution model simulations forced by GIA predictions replicate this recorded eastward diversion (Pico et al., 2018b).

In the lower reaches of the Delaware River (0–65 km upstream of the modern coastline), modeled transport capacity Q_c is reduced by ~ 10 –98% (Fig. 4C). Our predictions of Q_c reductions are in line with observations of increased aggradation from 40–25 ka in the lower reaches of the Delaware (Stanford et al., 2016). Our modeling indicates a reversed slope may have occurred in the Delaware from 20–35 km upstream of the modern coastline, which supports the suggestion that GIA-induced slope changes, in conjunction with increased aggradation, might have reversed local channel slope and induced a major avulsion (Stanford et al., 2016). Confirming an eastward diversion of the Delaware River near Trenton into the Raritan drainage basin will require additional data such as provenance studies on sediment cores near the mouth of the Raritan.

4.5. The Susquehanna and Potomac Rivers

Modeled changes in transport capacity Q_c peak at various locations along the Potomac River (Fig. 4C), coinciding with regions where the slope steepened (Fig. 4A) as the channel crosses a gradient in the GIA-induced crustal deformation field (Fig. 1A). Modeled Q_c increased by 360% at this peak, resulting in a more than doubling of the sediment transport capacity. Erosion rates measured ~ 25 km upstream of the modern coastline show that incision rates from 33 to 13 ka increased by at least a factor of two relative to those in the period 85–33 ka (Reusser et al., 2004). To the extent that increases in sediment transport capacity imply an increased tendency for river incision, our model is consistent with this accelerated incision in the Potomac.

The modeled transport capacity Q_c in the Susquehanna increases from 36 to 20 ka in a stretch along the lower reaches (beginning 80 km upstream of the modern coastline) and decreases in its upper reaches (Fig. 4C). Nevertheless, the region where transport capacity more than doubles (warm colors) does not coincide with the location 35 km upstream of the modern shoreline where measurements indicate an incisional pulse (Reusser et al., 2006). At this location, our model shows no change in Q_c (Fig. 4). Our simulations suggest that a mechanism other than GIA, such as melt-water associated with the glaciated region of the Susquehanna, may be responsible for the observed increase in erosion rates from 30–14 ka.

To investigate other possible explanations for the differing responses of the Potomac and Susquehanna, we consider regional factors that could have influenced both drainage basins, including the time-dependent response to base level fall and changes in precipitation. We calculate the transit time, τ for a knickpoint to

propagate from base level to a distance x upstream as (Royden and Perron, 2013; Goren, 2016)

$$\tau(x) = \int_0^x \frac{dx'}{kA(x')^m} \quad (3)$$

In solving this equation, we use $k = 2.5 \times 10^{-6} \text{ yr}^{-1}$ and $m = 0.5$, as in Miller et al. (2013), and the parameter x is the along-channel distance upstream of the modern shoreline. Following this approach, we estimate a value for τ of 50 ky for the Potomac at a location 25 km upstream from the modern coastline, and 33 ky for the Susquehanna at a location 35 km upstream of the modern coastline (Appendix Fig. A.4). Thus, for this value of k , if knickpoints had been generated at the coast at the LGM (26 ka), they should still be downstream of the locations of accelerated incision on the Potomac and Susquehanna, implying that propagation of coastally-generated knickpoints could not have driven the observed changes in incision rate. We stress, however, that if the relevant k value for the lower reaches of these rivers were higher than the one we applied by a factor of 3–5, or if knickpoint propagation were accelerated by factors not accounted for in the stream power law (e.g., changes in sediment supply or grain size), then knickpoints could have propagated past the locations of accelerated incision within the relevant time window, implying that the observed changes in incision rate could have been generated by knickpoint propagation.

Another argument against knickpoint-driven accelerated incision is that the coastal topography is not conducive to generating knickpoints. The continental shelf offshore of these modern-day river mouths in Chesapeake Bay is broad and low-gradient, such that even a large fall in local sea level would result in a relatively small vertical perturbation in the river profile. Large knickpoints are thus unlikely to form at these river mouths, even under large changes in sea level.

We consider it less likely that the observed increases in river incision were caused by changes in river water discharge. If bedrock river incision, the mechanism inferred for both the Potomac and Susquehanna Rivers, scales with the square root of basin-averaged precipitation rate, as previous studies suggest (e.g., Ferrier et al., 2013), then the observed doubling in river incision rate would require precipitation to have quadrupled. Pollen records and global circulation models, however, suggest that the U.S. mid-Atlantic was cooler and drier leading into the Last Glacial Maximum than during the Holocene (Leigh et al., 2004), and thus river water discharge was likely lower.

Although our analysis is consistent with the hypothesis that GIA-induced crustal deformation influenced the evolution of several US mid-Atlantic rivers substantially, additional factors beyond those considered here could have altered patterns of channel incision and aggradation. The extent and location of ice and permafrost could have altered erosion rates and processes in rivers, as well as affecting sediment supply (Herman et al., 2011; West et al., 2013). Furthermore, calculating sediment transport capacity in glaciated regions would require considering different laws for erosion and sediment transport. In our study area, this is particularly relevant for the Hudson, Delaware, and Susquehanna rivers, which were either almost entirely glaciated (Hudson) or glaciated in their northern halves (Delaware and Susquehanna) at the LGM (Fig. 1B). The transient response of channels to GIA-induced uplift could include adjustments in channel width or sinuosity, which could influence the sensitivity of channels to changes in slope or drainage area. For example, an increase in bed shear stress due to an increase in drainage area (and therefore water discharge) or slope might be buffered by channel widening or enhanced by channel narrowing (Yanites, 2018). Our parameterization of sediment flux

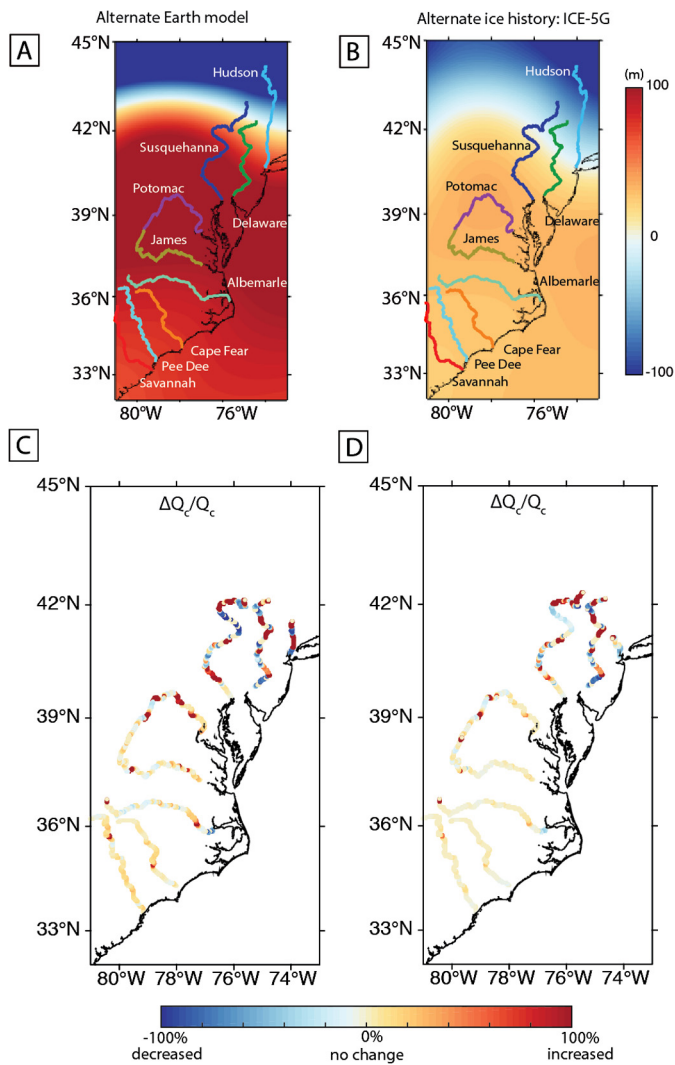


Fig. 5. Topographic change from 36 to 20 ka predicted using an alternate Earth model (A) or ice history ICE-5G (B). Percent change in transport capacity using alternate Earth model (C) and alternate ice history ICE-5G (D).

in terms of drainage area implicitly includes a dependence of channel width on water discharge, but it does not capture all possible aspects of a channel's transient width adjustment. Sinuosity effects on sediment transport capacity would likely work in the same direction as changes to channel slope (Rosgen, 1994). For example, a reduction in slope might cause sinuosity to increase, which should further reduce slope and transport capacity, causing a trend toward faster deposition or slower erosion.

4.6. Sensitivity to Earth and ice models

Modeled crustal deformation using GIA simulations are sensitive to the choice of ice history and Earth viscosity structure. We assess the sensitivity of our results to these model inputs by considering an alternate Earth model and ice history. In particular, we adopt an Earth structure characterized by upper and lower mantle viscosities of 0.2×10^{21} Pa s and 5×10^{22} Pa s, respectively, i.e., a model with a weaker upper mantle and stiffer lower mantle relative to the Earth model adopted in simulations shown in Fig. 1 (Fig. 5A). Predicted percent slope change (and transport capacity) are of larger magnitude using this Earth model, but trends in each river are similar (Fig. 5C; Appendix Fig. A.5).

We assess the sensitivity of our results to the selected ice history by performing GIA simulations with ice history ICE-5G (Peltier

and Fairbanks, 2006). In the ICE-5G ice history (Fig. 1B), the Laurentide Ice Sheet grows steadily over the glacial phase such that by 36 ka, the predicted topography is largely in isostatic equilibrium (Fig. 5B). In this case, we find that the predicted changes in channel slope and transport capacity are minor for most rivers. The Delaware and Susquehanna Rivers are exceptions to this general trend (Fig. 5D; Appendix Fig. A.6). The Delaware is predicted to have a reduction in Q_c (Fig. 5D), similar to the results using ice history ICE-PC2 (Fig. 4C). In contrast to the results in Fig. 4, the Potomac shows no change to Q_c (Fig. 5D). Similarly, the Susquehanna shows no change to Q_c at the location of observation (Fig. 5D). To the extent that changes in Q_c indicate changes in erosion and deposition, the topographic changes predicted using ICE-5G are consistent with the observed aggradation in the Delaware, but are not consistent with the observed incision in the Potomac.

The improved fit with the Potomac observations of the ICE-PC2 history, used in the main results and constrained by sea-level records along the U.S. mid-Atlantic, supports an increasing body of evidence for a rapidly growing eastern Laurentide Ice Sheet, beginning ~50–35 ka (Carlson et al., 2018; Dalton et al., 2019, 2016; Pico et al., 2017). In this study, we have shown that a rapidly uplifting peripheral bulge produces predictions of river dynamics consistent with observations in the Delaware and Potomac. A rapidly uplifting peripheral bulge is also supported by prior work which showed that the crustal deformation associated with ice history ICE-PC2 is more consistent with the eastward diversion of the Hudson River than previously published ice histories. The conjunction of these results points to the potential of ancient landscapes to serve as an additional constraint on crustal deformation associated with ice loading, which can, in turn, be used to differentiate between possible past ice sheet histories.

5. Conclusion

In this study, we explored the impact of the Laurentide peripheral bulge growth on rivers along the U.S. mid-Atlantic during the last glacial cycle. Our GIA simulations produced crustal deformation rates on the order of 10 mm/yr along the U.S. mid-Atlantic during the phase of peripheral bulge growth near the end of the last glaciation. Using this GIA model, we calculated changes to river channel slope and drainage area over the time period of particularly rapid peripheral bulge growth (36–20 ka) and used these changes to calculate perturbations to sediment transport capacity or bedrock incision rate in river channels. We then explored connections between these model calculations and previously documented transitions in river dynamics in the Hudson, Delaware, Susquehanna, and Potomac Rivers during the interval of peripheral bulge growth. Assuming that sediment supply did not change significantly over this time, we found that GIA-driven changes in sediment transport capacity or bedrock incision rate are consistent with the observed patterns of aggradation in the Delaware, incision in the Potomac, and a diversion in the Hudson River, but are inconsistent with an erosional pulse observed in the Susquehanna. Our analyses add to a growing body of evidence showing that GIA-induced crustal deformation can drive river evolution over millennial timescales.

Acknowledgements

We appreciate thoughtful discussions with P. Bierman, which improved the content of this manuscript. T.P. acknowledges funding from NSF-GRFP. T.P. and J.X.M. acknowledge funding from Harvard University. J.T.P. thanks Harvard University for a sabbatical stay. K.L.F. acknowledges support from NSF grant EAR-1525922 and ACS-PRF grant 58209-DNI8.

Appendix A

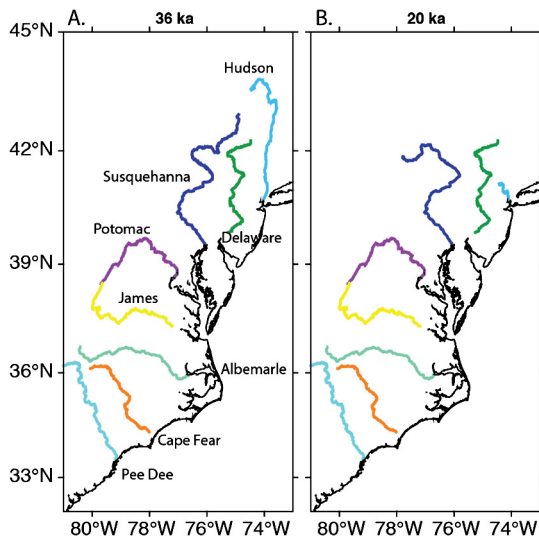


Fig. A.1. River channel locations at 36 ka (A) and at 20 ka (B). Black line shows modern coastline.

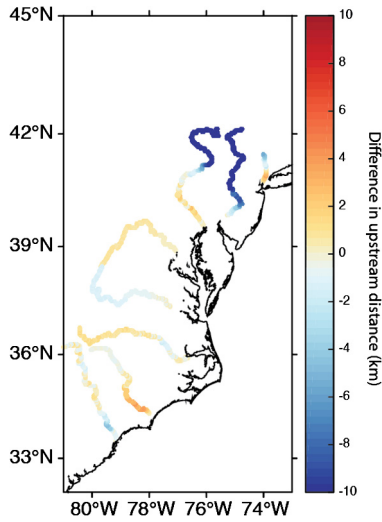


Fig. A.2. Difference in upstream distance measured from modern coastline in river channels between 36 and 20 ka, where upstream distance for 20 ka channels was subtracted from the upstream distance along 36 ka channels.

Table A.1

Drainage area for river systems highlighted in Fig. 2 at 36 ka and 20 ka. Drainage areas are calculated at the 36 ka shoreline predicted from GIA simulations driven by the ice history ICE-PC2.

| River | 36 ka drainage area (km ²) | 20 ka drainage area (km ²) |
|-------------|--|--|
| Hudson | 5.3×10^4 | 1.1×10^4 |
| Delaware | 4.25×10^4 | 4.1×10^4 |
| Susquehanna | 10.1×10^4 | 9.4×10^4 |
| Potomac | 4.8×10^4 | 4.8×10^4 |
| James | 3.5×10^{10} | 3.4×10^4 |
| Albemarle | 6.3×10^4 | 6.2×10^4 |
| Cape Fear | 3.0×10^4 | 2.9×10^4 |
| Pee Dee | 5.2×10^4 | 5.3×10^4 |
| Savannah | 2.6×10^4 | 2.7×10^4 |

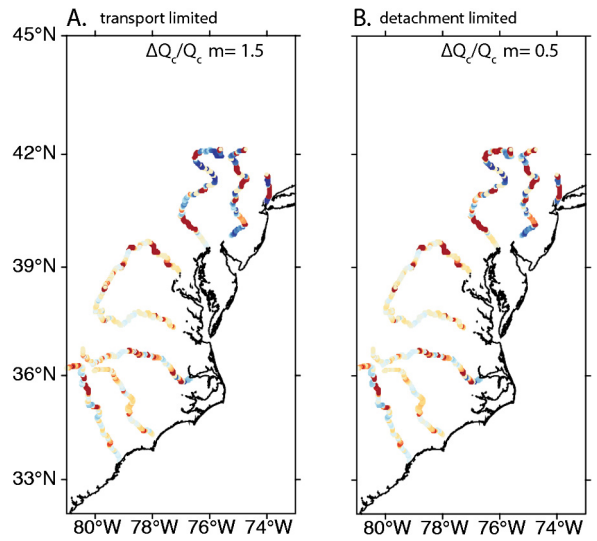


Fig. A.3. Modeled percent change in Q_c using $m = 1.5$, the case for transport-limited, (A), and using $m = 0.5$, as in main text, (B), the case for detachment-limited. Changes to Q_c in the transport-limited case are only substantially different from the detachment-limited case in rivers with significant changes in drainage area. Color-bar as in Fig. 4.

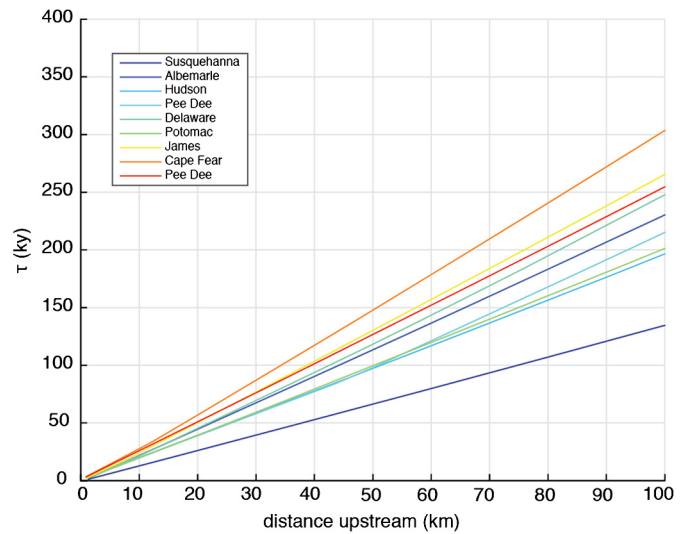


Fig. A.4. Calculated τ values, the transit time required for a knickpoint to propagate from base level to a distance x upstream, for each river system adopting $k = 2.5 \times 10^{-6}$ yr (2σ confidence interval from 2.08×10^{-6} /yr to 2.99×10^{-6} /yr) and $m = 0.5$, $n = 1$, as in Miller et al. (2013). Dotted lines show the upper and lower bound on the estimate of k values in Miller et al. (2013).

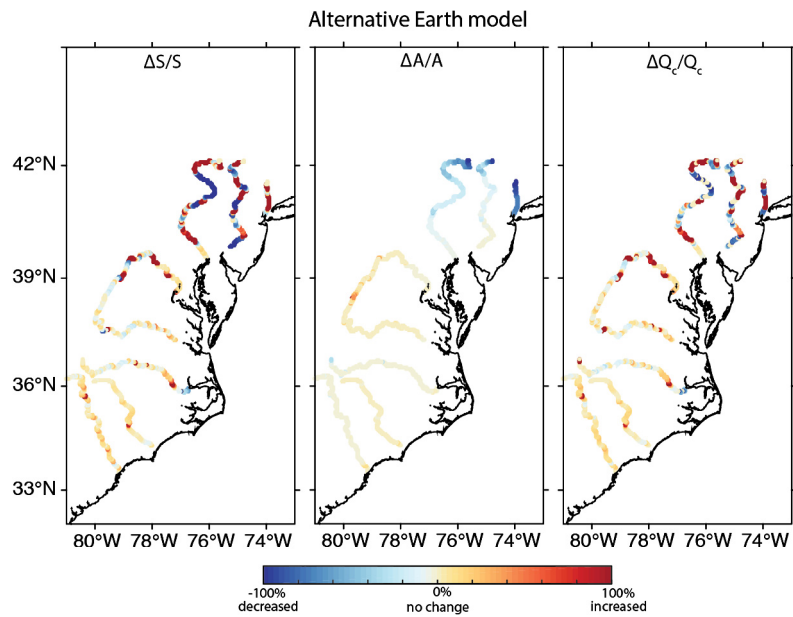


Fig. A.5. GIA-induced percent changes from 36 to 20 ka in (A) channel slope, (B) drainage area, and (C) transport capacity. Here GIA responses are governed by the alternate Earth model described in the main text (upper mantle: 0.2×10^{21} Pa s, lower mantle: 50×10^{21} Pa s).

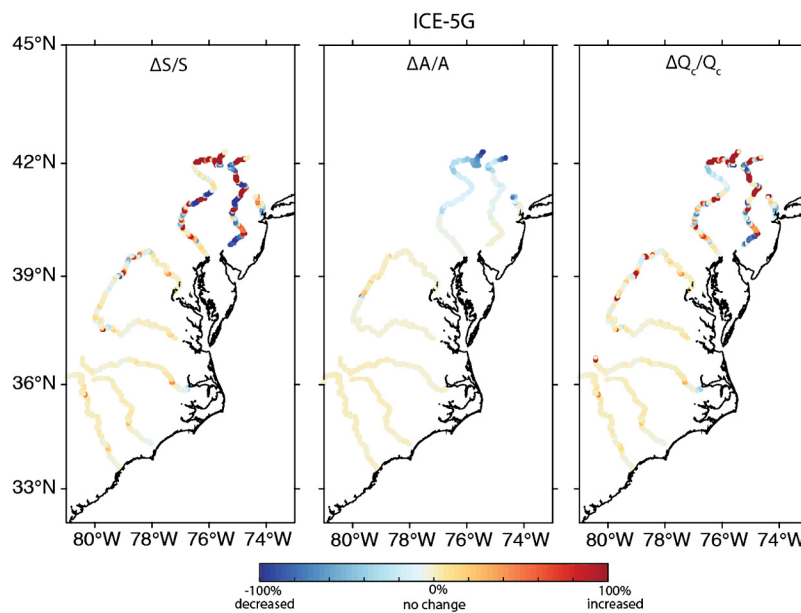


Fig. A.6. GIA-induced percent changes on the standard Earth model from 36 to 20 ka in (A) channel slope (B) drainage area and (C) sediment transport capacity Q_c , driven by the ice history ICE-5G.

References

- Barnes, R., Lehman, C., Mulla, D., 2014. Priority-flood: an optimal depression-filling and watershed-labeling algorithm for digital elevation models. *Comput. Geosci.* 62 (2), 117–127.
- Bierman, P., 2015. The incision history of the Great Falls of the Potomac River—The Kirk Bryan field trip. In: Geological Society of America, Field Guide, vol. 40, pp. 1–10.
- Carey, J.S., Sheridan, R.E., Ashley, G.M., Uptegrove, J., 2005. Glacially-influenced late Pleistocene stratigraphy of a passive margin: New Jersey's record of the North American ice sheet. *Mar. Geol.* 218 (1–4), 155–173. <https://doi.org/10.1016/j.margeo.2005.04.006>.
- Carlson, A.E., Tarasov, L., Pico, T., 2018. Rapid Laurentide ice-sheet advance towards southern last glacial maximum limit during marine isotope stage 3. *Quat. Sci. Rev.* 196, 118–123. <https://doi.org/10.1016/j.quascirev.2018.07.039>.
- Clark, P.U., Dyke, A.S., Shakun, J.D., Carlson, A.E., Clark, J., Wohlfarth, B., et al., McCabe, A.M., 2009. The last glacial maximum. *Science (N.Y.)* 325 (5941), 710–714. <https://doi.org/10.1126/science.1172873>.
- Creveling, J.R., Mitrovica, J.X., Clark, P.U., Waelbroeck, C., Pico, T., 2017. Predicted bounds on peak global mean sea level during marine isotope stages 5a and 5c. *Quat. Sci. Rev.* 163, 193–208. <https://doi.org/10.1016/j.quascirev.2017.03.003>.
- Dalton, A.S., Finkelstein, S.A., Barnett, P.J., Forman, S.L., 2016. Constraining the Late Pleistocene history of the Laurentide Ice Sheet by dating the Missinaibi Formation, Hudson Bay Lowlands, Canada. *Quat. Sci. Rev.* 146, 288–299. <https://doi.org/10.1016/j.quascirev.2016.06.015>.
- Dalton, A.S., Finkelstein, S.A., Forman, S.L., Barnett, P.J., Pico, T., Mitrovica, J.X., 2019. Was the Laurentide Ice Sheet significantly reduced during Marine Isotope Stage 3? *Geology* 47 (2), 111–114.
- Dyke, A.S., 2004. An outline of North American Deglaciation with emphasis on central and northern Canada. In: Ehlers, J., Gibbard, P.L. (Eds.), *Quaternary Glaciations—Extent and Chronology: Part II: North America*, pp. 373–424.
- Dyke, A.S., Andrews, J.T., Clark, P.U., England, J.H., Miller, G.H., Shaw, J., Veillette, J., 2002. The Laurentide and Innuitian Ice Sheet during the Last Glacial Maximum. *Quat. Sci. Rev.* 21, 9–31. [https://doi.org/10.1016/S0277-3791\(01\)00095-6](https://doi.org/10.1016/S0277-3791(01)00095-6).
- Ferrier, K.L., Huppert, K.L., Perron, J.T., 2013. Climatic control of bedrock river incision. *Nature* 496 (7444), 206–209. <https://doi.org/10.1038/nature11982>.

- Goren, L., 2016. A theoretical model for fluvial channel response time during time-dependent climatic and tectonic forcing. *Geophys. Res. Lett.* 1, 753–763. <https://doi.org/10.1002/2016GL070451>.
- Harel, M., Mudd, S.M., Attal, M., 2016. Global analysis of the stream power law parameters based on worldwide Be denudation rates. *Geomorphology* 268, 184–196. <https://doi.org/10.1016/j.geomorph.2016.05.035>.
- Herman, F., Beaud, F., Champagnac, J., Lemieux, J., Sternai, P., 2011. Glacial hydrology and erosion patterns: a mechanism for carving glacial valleys. *Earth Planet. Sci. Lett.* 310 (3–4), 498–508. <https://doi.org/10.1016/j.epsl.2011.08.022>.
- Howard, A.D., Dietrich, W.E., Seidl, M.A., 1994. Modeling fluvial erosion on regional to continental scales. *J. Geophys. Res.* 99.
- Howard, A.D., Kerby, G., 1983. Channel changes in badlands. *Bull. Geol. Soc. Am.* 94 (June), 739–752.
- Kendall, R.A., Mitrovica, J.X., Milne, G.A., 2005. On post-glacial sea level - II. Numerical formulation and comparative results on spherically symmetric models. *Geophys. J. Int.* 161 (3), 679–706. <https://doi.org/10.1111/j.1365-246X.2005.02553.x>.
- Knebel, H.J., Wood, S.A., Spiker, E.C., 1979. Hudson River: evidence for extensive migration on the exposed continental shelf during Pleistocene time. *Geology* 7 (May), 254–258.
- Lambeck, K., Purcell, A., Johnston, P., Nakada, M., Yokoyama, Y., 2003. Water-load definition in the glacio-hydro-isostatic sea-level equation. *Quat. Sci. Rev.* 22 (2–4), 309–318. [https://doi.org/10.1016/S0277-3791\(02\)00142-7](https://doi.org/10.1016/S0277-3791(02)00142-7).
- Lehner, B., Verdin, K., Jarvis, A., 2008. New global hydrography derived from spaceborne elevation data. *Eos* 89 (10), 93–94.
- Leigh, D.S., Srivastava, P., Brook, G.A., 2004. Late Pleistocene braided rivers of the Atlantic Coastal Plain, USA. *Quat. Sci. Rev.* 23, 65–84. [https://doi.org/10.1016/S0277-3791\(03\)00221-X](https://doi.org/10.1016/S0277-3791(03)00221-X).
- Massong, T.M., Montgomery, D.R., 2000. Influence of sediment supply, lithology, and wood debris on the distribution of bedrock and alluvial channels. *Geol. Soc. Am. Bull.* 5, 591–599.
- Miller, S.R., Sak, P.B., Kirby, E., Bierman, P.R., 2013. Neogene rejuvenation of central Appalachian topography: evidence for differential rock uplift from stream profiles and erosion rates. *Earth Planet. Sci. Lett.* 369–370, 1–12. <https://doi.org/10.1016/j.epsl.2013.04.007>.
- Milne, G.A., Mitrovica, J.X., 1996. Postglacial sea-level change on a rotating Earth: first results from a gravitationally self-consistent sea-level equation. *Geophys. J. Int.* 126 (3), F13–F20. <https://doi.org/10.1111/j.1365-246X.1996.tb04691.x>.
- Moucha, R., Forte, A.M., Mitrovica, J.X., Rowley, D.B., Quéré, S., Simmons, N.A., Grand, S.P., 2008. Dynamic topography and long-term sea-level variations: there is no such thing as a stable continental platform. *Earth Planet. Sci. Lett.* 271, 101–108. <https://doi.org/10.1016/j.epsl.2008.03.056>.
- Peltier, W.R., Fairbanks, R.G., 2006. Global glacial ice volume and Last Glacial Maximum duration from an extended Barbados sea level record. *Quat. Sci. Rev.* 25, 3322–3337. <https://doi.org/10.1016/j.quascirev.2006.04.010>.
- Pico, T., Creveling, J.R., Mitrovica, J.X., 2017. Sea-level records from the U.S. mid-Atlantic constrain Laurentide Ice Sheet extent during Marine Isotope Stage 3. *Nat. Commun.* 8 (May), 15612. <https://doi.org/10.1038/ncomms15612>.
- Pico, T., Birch, L., Weisenberg, J., Mitrovica, J.X., 2018a. Refining the Laurentide Ice Sheet at Marine Isotope Stage 3: a data-based approach combining glacial isostatic simulations with a dynamic ice model. *Quat. Sci. Rev.* 195, 171–179. <https://doi.org/10.1016/j.quascirev.2018.07.023>.
- Pico, T., Mitrovica, J.X., Braun, J., Ferrier, K.L., 2018b. Glacial isostatic adjustment deflects the path of the ancestral Hudson River. *Geology* 7, 1–4.
- Pico, T., Mitrovica, J.X., Ferrier, K.L., Braun, J., 2016. Global ice volume during MIS 3 inferred from a sea-level analysis of sedimentary core records in the Yellow River Delta. *Quat. Sci. Rev.* 152, 72–79. <https://doi.org/10.1016/j.quascirev.2016.09.012>.
- Potter, E.K., Lambeck, K., 2003. Reconciliation of sea-level observations in the Western North Atlantic during the last glacial cycle. *Earth Planet. Sci. Lett.* 217 (1–2), 171–181. [https://doi.org/10.1016/S0012-821X\(03\)00587-9](https://doi.org/10.1016/S0012-821X(03)00587-9).
- Reusser, L., Bierman, P., Pavich, M., Larsen, J., Finkel, R., 2006. An episode of rapid bedrock channel incision during the last glacial cycle, measured with ^{10}Be . *Am. J. Sci.* 306 (February), 69–102.
- Reusser, L.J., Bierman, P., Finkel, R., Bierman, P.R., Pavich, M.J., Zen, E., 2004. Rapid late Pleistocene incision of Atlantic passive-margin river gorges of Atlantic passive-margin. *Science* 305 (July). <https://doi.org/10.1126/science.1097780>.
- Rosgen, D.L., 1994. A classification of natural rivers. *Catena* 22, 169–199.
- Royden, L., Perron, J.T., 2013. Solutions of the stream power equation and application to the evolution of river longitudinal profiles. *J. Geophys. Res., Earth Surf.* 118 (May), 497–518. <https://doi.org/10.1002/jgrf.20031>.
- Seidl, M.A., Dietrich, W.E., 1992. The problem of channel erosion into bedrock. In: *Functional Geomorphology*, pp. 101–124.
- Sklar, L.S., Dietrich, W.E., 2001. Sediment and rock strength controls on river incision into bedrock. *Geology* 29 (12), 1087–1090.
- Sklar, L.S., Dietrich, W.E., 2004. A mechanistic model for river incision into bedrock by saltating bed load. *Water Resour. Res.* 40, 1–22. <https://doi.org/10.1029/2003WR002496>.
- Snyder, N.P., Whipple, K.X., Tucker, G.E., Merritts, D.J., 2003. Importance of a stochastic distribution of floods and erosion thresholds in the bedrock river incision problem. *J. Geophys. Res.* 108 (B2), 2117. <https://doi.org/10.1029/2001JB001655>.
- Stanford, S.D., Witte, R.W., Braun, D.D., Ridge, J.C., 2016. Quaternary fluvial history of the Delaware River, New Jersey and Pennsylvania, USA: the effects of glaciation, glacioisostasy, and eustasy on a proglacial river system. *Geomorphology* 264, 12–28. <https://doi.org/10.1016/j.geomorph.2016.04.002>.
- West, N., Kirby, E., Bierman, P., Slingerland, R., Ma, L., Rood, D., Brantley, S., 2013. Regolith production and transport at the Susquehanna Shale Hills Critical Zone Observatory, part 2: insights from meteoric ^{10}Be . *J. Geophys. Res., Earth Surf.* 118, 1877–1896. <https://doi.org/10.1002/jgrf.20121>.
- Whipple, K.X., 2004. Bedrock rivers and the geomorphology of active orogens. *Annu. Rev. Earth Planet. Sci.* <https://doi.org/10.1146/annurev.earth.32.101802.120356>.
- Whipple, K.X., Tucker, G.E., 1999. Dynamics of stream-power river incision model. *J. Geophys. Res.* 104 (August), 661–674.
- Whipple, K.X., Tucker, G.E., 2002. Implications of sediment-flux-dependent river incision models for landscape evolution. *J. Geophys. Res.* 107.
- Whitehouse, P.L., Allen, M.B., Milne, G.A., 2007. Glacial isostatic adjustment as a control on coastal processes: an example from the Siberian Arctic. *Geology* 35 (8), 747. <https://doi.org/10.1130/G23437A.1>.
- Wickert, A.D., 2016. Reconstruction of North American drainage basins and river discharge since the Last Glacial Maximum. *Earth Surf. Dyn.* 4 (4), 831–869. <https://doi.org/10.5194/esurf-4-831-2016>.
- Wickert, A.D., Anderson, R.S., Mitrovica, J.X., Naylor, S., Carson, E.C., 2019. The Mississippi River records glacial-isostatic deformation of North America. *Sci. Adv.* (January), 1–8.
- Willgoose, G., Bras, R.L., Rodriguez-Iturbe, I., 1991. A coupled channel network growth and hillslope evolution model 1. Theory. *Water Resour. Res.* 27 (7), 1671–1684.
- Yanites, B.J., 2018. The dynamics of channel slope, width, and sediment in actively eroding bedrock river systems journal of geophysical research: Earth surface. *J. Geophys. Res., Earth Surf.*, 1504–1527. <https://doi.org/10.1029/2017JF004405>.